IET Generation, Transmission & Distribution

Research Article

IET Journals
The Institution of Engineering and Technology

Real-time estimation of ATC using PMU data and ANN

ISSN 1751-8687
Received on 16th August 2019
Revised 20th May 2020
Accepted on 2nd June 2020
E-First on 7th July 2020
doi: 10.1049/iet-gtd.2019.1260
www.ietdl.org

Devesh Shukla[1], *S.P. Singh*[1] ✉

[1]*Department of Electrical Engineering, IIT(BHU) Varanasi, India*

✉ *E-mail: spsingh.eee@itbhu.ac.in*

Abstract: An artificial neural network (ANN) architecture for real-time estimation of available transfer capability (ATC) has been reported in this study. The real-time data obtained from phasor measurement unit (PMU) is utilised to generate target output (ATC) using the pattern search optimisation-based method. The set of information provided as input to the pattern search-based ATC optimiser along with its output forms the input and target output for ANN training. The input information consists of active and reactive power injected along with voltage and current vectors measured at PMU buses. The ATC optimiser is functional as long as ANN is under training. Once the ANN is trained, it receives input set directly from PMU and produces ATC values. PMU emulation is employed for archiving the PMU data. The proposed method is tested on modified IEEE 24-bus, IEEE 30-bus, and IEEE 118-bus test system. The proposed method has also been implemented on real-time digital simulator.

Nomenclature

B	represent set of all buses in the system
Gen	set representing the subset of generators in the system
Ld	set representing all the load buses in the system
n_{sink}	number of load buses in sink area.
l	subset of "Ld" representing all the load buses in the sink area
s	subset of Gen representing gen buses in source area.
x_i	load at the ith bus
x_{oi}	initial load at the ith bus.
$x_{\min}$	lower limit of the variable
ψ	pattern set
ϕ_i	the ith pattern vector of pattern set
ϕ_i^l	the lth component of the ith pattern vector
ϕ_i'	transpose of ϕ_i
ζ	mesh size
P_{gi}	active power injected at the ith bus
P_{di}	active power drawn at the ith bus
Q_{gi}	reactive power injected at the ith bus
Q_{di}	reactive power drawn at the ith bus
P_{ij}	power flowing in line connecting buses i,j
$P_{ij}^{\max}$	maximum permissible power flow through lines i, j
$Q_{gi}^{\max}$	upper limit of reactive power generation of the ith generator
$Q_{gi}^{\min}$	lower limit of reactive power generation of the ith generator
V_i	voltage of the ith bus
$V_i^{\min}$	lower limit of voltage permissible at the ith bus
$V_i^{\max}$	upper limit of voltage permissible at the ith bus
N	total number of buses in the system
M	total number of generator buses
L	total number of lines
GTNET	giga-transceiver network communication card
SKT	socket protocol
GTSYNC	synchronisation card

1 Introduction

The developments which recently took place in power system structure namely deregulation and open access coupled with the increased integration of renewable sources of generation added to the complexity of operation and control of the power system. This added complexity increased the significance of available transfer capability (ATC) determination. Conventionally, the ATC is pre-computed at any instant of time depending upon the load forecasting information, availability of generating units and transmission lines, existing transmission commitments, and transmission reliability margin. Under current practices, the total transfer capability (TTC)/ATC is projected much before the actual operation. In actuality, the TTC/ATC at the current operating point might be different from those predicted TTC/ATC. However, such an operation would not result in the optimal utilisation of available resources, and optimal operation of the power system. The availability of information regarding real-time ATC would be of great use to the power system operator. Such information would also allow short time open access either for generating entities or consumers. The issue of ATC calculations has been addressed extensively in the literature [1–3].

The deployment of modern measuring and communication devices across the power grid has made the real-time measurements of states of the power system feasible [4]. Phasor measurement unit (PMU) measurements can be used for real-time monitoring and analysis of the power system. Wide-scale research activities are being done on enhancing the power system operation and control while using the measurements obtained from the PMUs [5–7]. The measurement-based technique provides a snapshot of the system in terms of the measured variables. The predictive/preventive/control action can be taken as and when required, taking into cognizance of the measured variables.

Transparency in information pertinent to ATC entails regular evaluation of ATC. Overestimated ATC would cause excessive transactions of power, thereby hampering the security of the system. On the contrary, underestimated ATC would cause inadequate power transactions, which would affect the market economy adversely. Therefore, mitigation of the undesirable impact of open access to energy markets would require a clear indication regarding the ATC of the system. Several methods for determination of ATC have been proposed in the literature such as sensitivity factor-based methods [8, 9] continuation power flow-based methods [10], and optimum power flow-based methods [11]. Optimisation techniques based methods have been investigated in [12, 13] where artificial fish swarm optimisation and particle swarm optimisation techniques have been used in ATC calculation, respectively. A pattern search algorithm-based method for offline ATC estimation has been discussed in [14]. ATC evaluation using

probabilistic approaches has also been investigated in [15]. Application of neural network for ATC determination has also been proposed in the literature [16–19]. In [20] measurement-dependent injection distribution factors-based method in which synchrophasor measurements have been utilised for ATC estimation. The ATC evaluation considering correlated wind power integration have been presented in [21]. The ATC evaluation taking AC-DC power flow into consideration have been done in [22]. Assessment of ATC probabilistically by using optimal condition decomposition technique and latin hypercube sampling (LHS) for the power system in the presence of wind energy sources has been discussed in [23]. An in-depth review of ATC evaluation methods could be found in [24]. In this study, real-time estimation of ATC using PMU data and artificial neural network (ANN) has been proposed. The proposed method could be utilised in real-time for estimating the ATC of the system. At first, a method for offline training of ANN-based estimator using pseudo-PMU (PPMU) emulator has been discussed. The PPMU emulator could archive and provide the PMU data in an offline environment for training and testing of ANN-based ATC estimator. The ATC values for training estimators have been obtained using a pattern search-based optimisation technique. The major contributions of the present study are enumerated as follows.

- A method for real-time estimation of ATC by employing measurement data from PMU.
- A PMU emulator (PPMU) for obtaining the data required for training and testing of the ANN-based real-time estimator.
- Feature extraction for ATC estimation using sparse filter algorithm has been proposed for reducing the size of input features.
- Feasibility of real-time applicability of the proposed method has been authenticated by its implementation on real-time digital simulator (RTDS)

The paper has been divided into eight different sections where Section 1 gives the introduction, Section 2 defines ATC and presents a pattern search optimisation-based technique for estimation of ATC. In Section 3, PMU and its emulation for static and quasi-static analysis using PPMU are discussed. Section 4 presents the linear state estimator (LSE) using weighted least square. The real-time estimation of ATC using ANN has been discussed in Section 5. Section 6 discusses the implementation of the method. Case studies and results are discussed in Sections 7, and 8 concludes the work.

2 ATC definition and evaluation

The power that could be delivered in addition to the existing transmission commitments with due adherence to the transmission reliability margin (TRM) and capacity benefit margin (CBM) has been defined as ATC [4]. Mathematically

$$\text{ATC} = \text{TTC} - (\text{CBM} + \text{TRM}) - \text{ETC} \tag{1}$$

In (1), CBM and TRM depend on the system states and methods employed for their evaluation. ATC is significant for both economic, as well as operational aspects of the power system. As far as the economy is concerned, the adequate information of ATC would allow the maximum transaction of power, in-turn resulting in revenue maximisation and ensuring the system security simultaneously.

2.1 Problem formulation

The value of TTC in (1) can be obtained by maximising the demand in the sink area of the system, expressed mathematically as

$$\max\ (f(x)) \tag{2}$$

where

$$f(x) = \sum_{i=1}^{n_{\text{sink}}} x_i - \sum_{i=1}^{n_{\text{sink}}} x_{0i} \tag{3}$$

The objective function expressed by (3) is a representative of maximising the loading at all the buses contained in l without disturbing the loading at all the other load buses (i.e. Ld $\cap$ l' buses). If the increment in the loading is not adequately addressed by the corresponding increment in a generation, the generation load balance would be disturbed. Therefore, the increment in load is provided by incrementing the proportional generation in s. Once the TTC value is obtained, the ATC is determined by deduction of the CBM, TRM, and existing transmission commitments (ETC) from the TTC value.

2.1.1 Equality constraints: The problem objective is to be met fulfilling the power balance expressed as

$$\sum_{i=1}^{M} P_{gi} - \sum_{i=1}^{N} P_{di} - \sum_{i=1}^{N}\sum_{j=1}^{N} V_i V_j Y_{ij} \cos(\theta_{i,j} - \delta_i + \delta_j) = 0 \quad i, j \in 1, 2, \ldots, N \tag{4}$$

and

$$\sum_{i=1}^{M} Q_{gi} - \sum_{i=1}^{N} Q_{di} - \sum_{i=1}^{N}\sum_{j=1}^{N} V_i V_j Y_{i,j} \sin(\theta_{i,j} - \delta_i + \delta_j) = 0 \quad i, j \in 1, 2, \ldots, N \tag{5}$$

2.1.2 Inequality constraints: To ensure that the system remains in healthy operating conditions at the optimum solution, the line flows through the lines, active and reactive power generation of the generators and voltage magnitude at each bus remain well within their limits. to ensure these conditions, the following inequality constraints are to be maintained:

$$P_{gi}^{\min} \le P_{gi} \le P_{gi}^{\max}; \quad i \in 1, 2, \ldots, M \tag{6}$$

$$Q_{gi}^{\min} \le Q_{gi} \le Q_{gi}^{\max}; \quad i \in 1, 2, \ldots, M \tag{7}$$

$$V_i^{\min} \le V_i \le V_i^{\max}; \quad i \in 1, 2, \ldots, N \tag{8}$$

$$P_{ij}^{\min} \le P_{ij} \le P_{ij}^{\max}; \quad i \in 1, 2, \ldots, N \tag{9}$$

For defining the domain of investigation, a maximum loading of the sink area is defined as the upper limit of independent variable x, while the base case values are taken as the lower limits say

$$x_{\min} \le x \le x_{\max} \tag{10}$$

In this work, the system considered for ATC estimation has been divided into several areas and ATC for power transactions between any two areas (considered at a time) has been estimated. Among these two areas, one area is considered as a source while the other area as a sink, and the ATC has been evaluated for power transfer from generators in the source area to loads in the sink area. It is to be mentioned that source area loads and sink area generator's power have been considered constant while evaluating ATC. The ATC computation and analysis have been carried out for a particular loading condition using the pattern search optimisation. The optimisation process involves increasing the loads in the sink area that have been compensated through incrementing the generators in the source area. The power factor of the loads has been maintained constant to ensure that the load characteristics are preserved.

2.2 Generation of loading pattern

The technique used for generating training and testing data using the offline ATC evaluation process is schematically shown in the flowchart of Fig. 1. Initially, the loading in the sink area of the

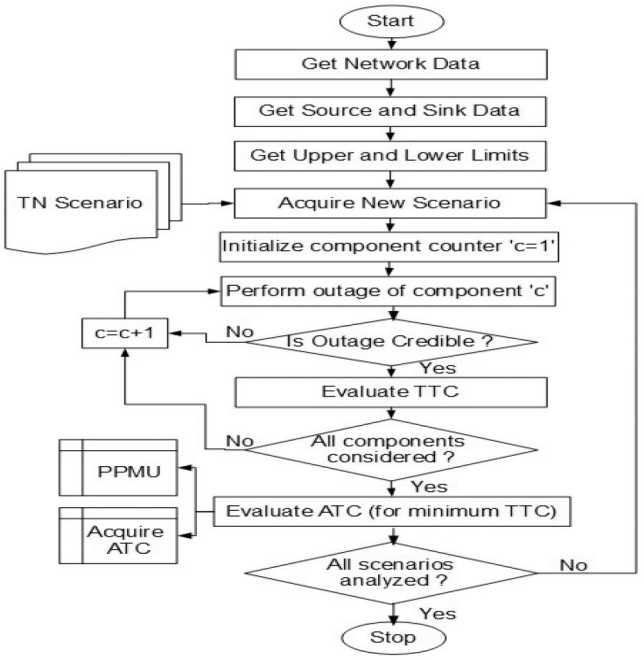

Fig. 1 *Flowchart of offline ATC evaluation and training data generation*

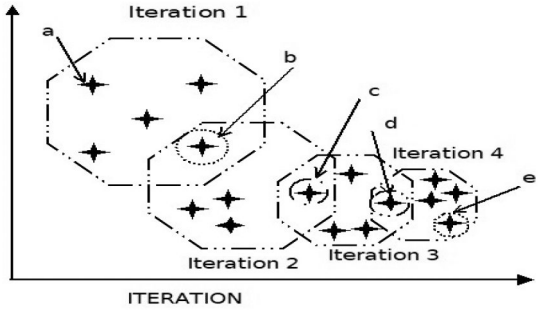

Fig. 2 *Pattern search optimisation process*

network under consideration has been considered as a lower limit (lb), while the upper limit (ub) has been taken as the maximum loading limit of load buses. Pattern search (PS) has been employed for generating different loading conditions, solutions for which have been obtained with the help of Newton Raphson method. The objective function has been evaluated only for the convergent points as those points represent the feasible solution. The process is continued until the termination criterion (an indicator of optimal/ near-optimal solution) is met.

2.3 Optimisation technique for solution

The optimisation of the problem is accomplished by employing a pattern search optimisation technique [25–27]. PS optimisation being a direct search optimisation, in its process the information pertinent to the gradient of the objective function is not required [25].

2.3.1 Patterns: The cardinality of the objective function's independent variables defines the number of patterns used in the PS. Nascent patterns in the optimisation process are generated using the generalised pattern search algorithm. For instance, pattern set ψ, for vector x_0 (initial point) with l components would be

$$\begin{aligned}[\psi]_{l*n^*} &= [\varphi_1', \varphi_2', \varphi_3', \ldots, \varphi_{n^*}']_{l*n^*} \\ [\varphi_i]_{1*l} &= [\varphi_i^1, \varphi_i^2, \ldots, , \varphi_i^l]_{1*l}\end{aligned} \tag{11}$$

In (11), n^* is $(l+1)$ if pattern (φ) is formed using minimal basis, else n^* is $(2\times l)$ when maximal basis is employed in pattern formation. For pattern search algorithm, two commonly used basis sets are maximal and minimal basis set. The pattern of vectors that forms these basis sets are fixed direction vectors. For example, if there are three independent variables in the problem (i.e. $l=3$), then for maximal basis the vectors $(2*l)$ would be formed as

$$\phi_1 = [1\ \ 0\ \ 0]; \quad \phi_2 = [0\ \ 1\ \ 0] \tag{12}$$

$$\phi_3 = [0\ \ 0\ \ 1]; \quad \phi_4 = [-1\ \ 0\ \ 0] \tag{13}$$

$$\phi_5 = [0\ \ -1\ \ 0]; \quad \phi_6 = [0\ \ 0\ \ -1] \tag{14}$$

for minimal basis the $(l+1)$ vectors would be formed as

$$\phi_1 = [1\ \ 0\ \ 0]; \quad \phi_2 = [0\ \ 1\ \ 0] \tag{15}$$

$$\phi_3 = [0\ \ 0\ \ 1]; \quad \phi_4 = [-1\ \ -1\ \ -1] \tag{16}$$

These vectors have been used to obtain the mesh.

2.3.2 Mesh: Mesh represents the set of points that are searched by the pattern search algorithm in each iteration. This search assists in finding a solution point that enhances the value of the objective function. A set of vectors d_j, produced by taking the product of patterns with the mesh size ζ, has been added to the optimal point of the previous iteration ($x_{\text{iter}-1}^{\text{optim}}$) to obtain the mesh points

$$\begin{aligned}d_j &= \zeta * \varphi_j' \\ D &= \zeta * \psi \\ x_{\text{iter}}^{\text{set}} &= x_{\text{iter}-1}^{\text{optim}} + D\end{aligned} \tag{17}$$

2.3.3 Polling: The process of computing the value of the objective function at each mesh point is called polling. Depending upon the outcome of the polls, the polling may be a successful poll or unsuccessful. The polling that results in the improvement of the optimal value has been considered as a successful poll. On the contrary, the one which does not yield improvement has been designated as an unsuccessful poll

$$\begin{aligned}x_{\text{iter}-1}^{\text{optim}} &\in x_{\text{iter}-1}^{\text{set}} \\ x_{\text{iter}}^{\text{optim}} &= \min \quad \mathcal{F}(x_{\text{iter}}^{\text{set}})\end{aligned} \tag{18}$$

2.3.4 Expanding and contracting: Updating the mesh size ζ during the solution process, after each poll, is referred to as expansion or contraction. The mesh size is updated by multiplying a constant higher (km) than (for a successful poll) or less (kl) than unity (for the unsuccessful poll).

$$\begin{aligned}&\text{if:} \quad x_{\text{iter}}^{\text{optim}} < x_{\text{iter}-1}^{\text{optim}} \\ &\zeta = km \times \zeta; \quad km > 1\text{expanding} \\ &\text{else} \quad \zeta = kl \times \zeta; \quad kl < 1\text{contraction}\end{aligned} \tag{19}$$

Convergence criterion for the optimisation could be specified by the maximum number of iteration, mesh size ζ, the time duration or change in objective function value (O.F). In the present work, mesh size ζ is taken as the termination criterion, i.e if the termination criterion is less than a pre-specified value then the optimisation process is terminated. In the present work, termination criterion of mesh size 1×10^{-15} has been taken. The schematic representation of the optimisation process has been shown in Fig. 2. The figure shows the pattern search process of two variable problems (for which four patterns are generated). The octagonal boundaries represent the mesh size, it can be seen that as the optimisation process proceeds and the solution approaches the optimal value the mesh size decrease. In iteration 1 (shown in the figure) the best function of the objective function is obtained corresponding to the pattern encircled by a circle, this point is selected and new patterns are generated around this pattern and this process continues until the termination criterion is met.

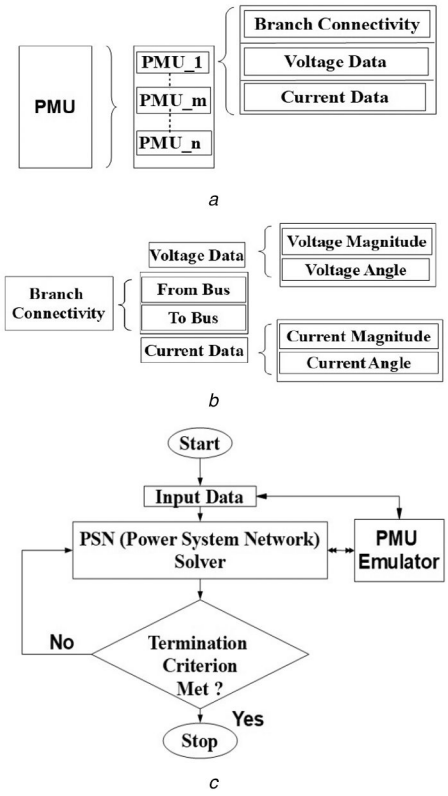

Fig. 3 *PMU storage layout*
(a) Overall layout, ***(b)*** Branch connectivity layout, ***(c)*** PMU emulation algorithm steps

2.4 Contingency screening

The ATC for any transaction is evaluated for any system such that in the event of occurrence any contingency $(N-1)$ the system remains within its operational limits. Therefore, contingency screening for identifying the critical contingencies (which are most sensitive to any given transaction) has to be performed. This has been achieved by using (20) [28]

$$\mathrm{PI}_c = \left[\sum_i \frac{d_{v,i}^u}{g_{v,i}^u}^{2e} + \sum_i \frac{d_{v,i}^l}{g_{v,i}^l}^{2e} + \sum_i \frac{d_{p,j}}{g_{p,j}}^{2e} \right] \tag{20}$$

$$d_{v,i}^u = \begin{cases} \dfrac{[V_i - f_i^u]}{V_i^d}; & \text{if} \quad V_i > f_i^u \\ 0; & \text{if} \quad V_i \le f_i^u \end{cases} \tag{21}$$

$$d_{v,i}^l = \begin{cases} \dfrac{[f_i^l - V_i]}{V_i^d}; & \text{if} \quad V_i > f_i^l \\ 0; & \text{if} \quad V_i \ge f_i^u \end{cases} \tag{22}$$

$$g_{v,i}^u = \frac{[V_i^u - f_i^u]}{V_i^d}$$
$$g_{v,i}^l = \frac{f_i^l - V_i^l}{V_i^d} \tag{23}$$

$$d_{p,j} = \begin{cases} \dfrac{[|P_j| - P_{f,j}]}{\mathrm{BaseMVA}}; & \text{if} \quad |P_j| > P_{f,j} \\ 0; & \text{if} \quad P_j \le P_{f,j} \end{cases} \tag{24}$$

$$g_{p,j} = \frac{[P_{p,j} - P_{f,j}]}{\mathrm{BaseMVA}} \tag{25}$$

Here, in the above equations, contingency index is PI_c, V_i and V_i^d are actual and desired voltage at the ith bus, f_i^u, f_i^l, V_i^u, V_i^l are the alarm limits and security limits. The parameters $d_{v,i}^u$, $d_{v,i}^l$, $g_{v,i}^u$, $g_{v,i}^l$ represent the normalised violations of upper and lower limits at the ith bus. $P_{f,j}$ and $P_{p,j}$ are the security and alarm limits for power flows in the jth line, respectively. The normalisation factor and normalised power flow limit violations for the jth line are $g_{p,j}$ and $d_{p,j}$ respectively. The value of e has been taken as 2, and it represents the exponent used in hyper ellipse equation [28]. The expression of the composite security index expressed in (20) has been used for contingency ranking. The severity of the contingency is governed by the PI_c value, higher the value of the index greater the severity. Now, TTC values corresponding to the selected critical contingencies have been evaluated and are arranged in increasing order of their value. The contingency for which the TTC value is minimum is selected as the most critical contingency for which ATC has to be evaluated.

3 PMU emulation

The PMU emulator reported in this study is capable of measuring the voltage magnitude and angle of the bus at which it is connected and the connecting branches' current magnitudes. Since it does not exhibit the entire/complete property of the PMU but measures above-mentioned parameters only, it is called PPMU. An interactive algorithm has been utilised to emulate the PPMUs that archive the relevant voltage and current information at the desired buses. The retrieved information is stored in fashion shown in Figs. 3*a* and *b*. The steps used to implement the emulation algorithm has been shown in Fig. 3*c*. in the form of aflow chart. Explanation of various stages in block diagram has been given below.

3.1 Input data

The input data is divided into two parts—fixed and variable. The fixed data consists of network parameters, number of PMUs, and their locations. While the variable data can be generated around the base case to obtain various operating conditions. Alternatively, if the forecasted load is available the same can be used to obtain base case generation information. Since the PMU emulation has been carried out for ATC evaluation, in the present work, the loading patterns need to be generated such that the loads and generations are simultaneously increased in the sink and source area, respectively.

3.2 PSN solver

The system states corresponding to the loading scenario mentioned above are obtained at this stage. For this purpose, the OPF solution using a decent gradient has been utilised. It is to be clarified that other methods of OPF could also be used in place of gradient search. However, for demonstration purpose, the gradient descent method has been utilised. The limits on active and reactive power generation of generating buses, voltage magnitude of load buses, and line flows have been taken care in the solution process.

3.3 PMU emulator

The PMU emulator interactively archives the voltage magnitudes, voltage angles, current magnitudes, and current angles produced by the PSN solver. In the PMU emulation stage, a stack of cells, as shown in Fig. 3*a* having cardinality equal to the installed number PMU's in the system, is formed. Each cell has been further segregated into three sub-cells. The information about branch connectivity is contained in the first sub-cell, which is further divided into two cells containing 'from bus' (branches originating from PMU bus) data and 'to bus' data (branches terminating at PMU bus). The second sub-cell stores the voltage magnitudes and voltage angles of the PMU buses, while the third sub-cell hosts the branch's current magnitudes and angles, as shown in Fig.3*b*.

If PPMU is not employed then an iterative algorithm that sweeps across the operating situations (probable/feasible solutions) and fetches the data if the bus id is the same as the PMU location bus would have to be utilised. This happens to be a time-consuming process and the time taken would increase with an

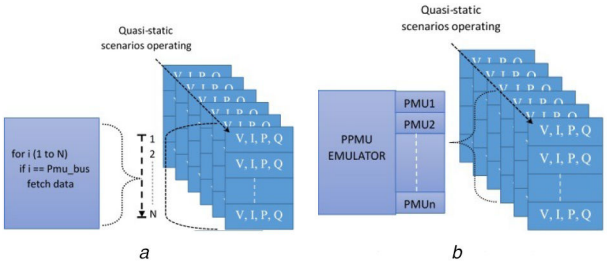

Fig. 4 *Schematic comparison of iterative and PPMU algorithms*
(a) Iterative algorithm, ***(b)*** PPMU algorithm

Table 1 Comparison of iterative and PPMU algorithm using MATLAB 17b on Intel i7 processor

Se No	Case	Time taken, s		
		Iterative algorithm	PPMU algorithm	Gradient descent OPF
1	IEEE 24-bus RTS	0.0011	0.0007	0.0465
2	IEEE 30-bus system	0.0012	0.0006	0.0548
3	IEEE 118-bus system	0.0043	0.0015	0.0780

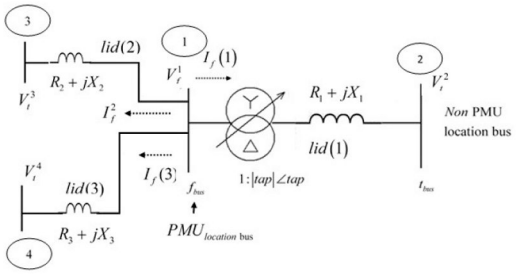

Fig. 5 *Illustrative example showing three buses connected to a PMU bus*

increase in complexity (number of buses) of the system. On the contrary, when PMU emulator is used in the ATC estimation framework then it interactively acquires the location of the PMU's in the network and directly acquires/fetches the data from operating situations (probable/feasible solutions). The schematic comparison of the iterative method and PPMU algorithm is shown in Fig. 4, whereas Table 1 gives the comparative results for the aforementioned methods on different test cases using MATLAB 17b running on an intel core i7 processor.

4 Linear state estimator

Linear state estimation is a substitute to conventional state estimation for real-time operation of the power system. Linear state estimation can be deployed to measure the voltage and current states of nodes where the PMUs are not placed, provided the PMU placement has been done for full observability of the network under consideration [29]. The problem formulation for linear state estimation can be mathematically expressed as

$$\text{Min} \quad \mathscr{R}^{\mathrm{T}}\boldsymbol{\mu}\mathscr{R}$$

$$\text{s.t.} \quad z = \begin{pmatrix} Z_1 \\ . \\ . \\ . \\ Z_m \end{pmatrix} = \mathscr{H}\boldsymbol{X} + \mathscr{R} = \begin{pmatrix} \mathscr{H}_{1,1} & \cdots & \mathscr{H}_{1,n} \\ \vdots & \ddots & \vdots \\ \mathscr{H}_{m,1} & \cdots & \mathscr{H}_{m,n} \end{pmatrix} \boldsymbol{X} + \begin{pmatrix} \mathscr{R}_1 \\ \vdots \\ \mathscr{R}_m \end{pmatrix} \tag{26}$$

where $\mathscr{R}$ is the error residue, $\boldsymbol{z}$ is the measured vector, $\boldsymbol{X}$ is the unknown vector, $\boldsymbol{\mu}$ is the weight matrix with all entries as real numbers and μ_i is the weight block for each measurement

$$\mu_i = \begin{pmatrix} \sigma^2_{z,\text{real}} & 0 \\ 0 & \sigma^2_{z,\text{imag}} \end{pmatrix} \tag{27}$$

The solution to the above state estimation is obtained without iteration

$$\boldsymbol{X} = (\mathscr{H}^{\mathrm{T}}\mu\mathscr{H})^{-1}\mathscr{H}^{\mathrm{T}}\boldsymbol{\mu z} \tag{28}$$

4.1 Formation of $\mathscr{H}$ matrix

The $\mathscr{H}$ matrix used in linear state estimation is obtained from the admittance matrix formed after the network information is archived and processed by the network topology processor. The dimension of the $\mathscr{H}$ matrix is $(m_{\mathrm{u}} \times m_{\mathrm{k}})$, where m_{u} is the number of unknown measurements and m_{k} is the number of known measurements. Let n_{b} be the number of buses at which PMUs are not placed and n_{p} be the buses at which the PMUs have been placed with n_{pb} being the number of branches connected at each bus. Now, $m_{\mathrm{u}} = n_{\mathrm{b}} - n_{\mathrm{p}}$ and $m_{\mathrm{k}} = n_{\mathrm{p}} + \sum_{i=1}^{i=n_{\mathrm{p}}} n_{\mathrm{pb}}(i)$. Fig. 5 illustrates an example of a four-bus interconnected network where bus 1 is the $\mathrm{PMU}_{\text{location bus}}$, line lid(1) with a tap changing transformer, and other lines connected to far end buses 2, 3, and 4. Now, the network admittance matrices are formed using

$$Y_{\mathrm{s}} = \frac{1}{R_{\mathrm{lid}} + \mathrm{j}X_{\mathrm{lid}}}; \quad Y_{\mathrm{tt}} = Y_{\mathrm{s}} + \frac{\mathrm{j}B_{\mathrm{c,lid}}}{2} \tag{29}$$

$$Y_{\mathrm{ff}} = \frac{Y_{\mathrm{tt}}}{\mathrm{tap} \times \mathrm{conj(tap)}}; Y_{\mathrm{ft}} = \frac{-Y_{\mathrm{s}}}{\mathrm{conj(tap)}}; Y_{\mathrm{tf}} = \frac{-Y_{\mathrm{s}}}{\mathrm{tap}} \tag{30}$$

$$Y_{\mathrm{F}} = \begin{bmatrix} Y_{\mathrm{ff}} & Y_{\mathrm{ft}} \\ Y_{\mathrm{tf}} & Y_{\mathrm{tt}} \end{bmatrix}; \quad Y_{\mathrm{T}} = \begin{bmatrix} Y_{\mathrm{tt}} & Y_{\mathrm{tf}} \\ Y_{\mathrm{ft}} & Y_{\mathrm{ff}} \end{bmatrix} \tag{31}$$

The voltage V_{f} and branch current I_{f} are known at the PMU location bus. This information can be used to obtain the information of far end bus using (32)

$$I_{\mathrm{ft}} = Y_{\mathrm{ff}}V_t + Y_{\mathrm{ft}}V_{\mathrm{f}}; \Rightarrow V_{\mathrm{t}} = \underbrace{\frac{I_{\mathrm{ft}}}{Y_{\mathrm{ff}}}}_{H_{\mathrm{ft}}} - \underbrace{\frac{Y_{\mathrm{ft}}V_{\mathrm{f}}}{Y_{\mathrm{ff}}}}_{H_{\mathrm{ff}}} \tag{32}$$

The measurement vector $\boldsymbol{Z}$ with size $(1 \times m_{\mathrm{k}})$ is obtained from the PPMU measurements as

$$\boldsymbol{Z} = \underbrace{\begin{bmatrix} \text{PPMU(1)} \cdot V \\ \text{PPMU(1)} \cdot I_{\mathrm{ft}^{\mathrm{l}}} \\ \text{PPMU(1)} \cdot I_{\mathrm{ft}^{\mathrm{nl}}} \\ \vdots \\ \text{PPMU(np)} \cdot V \\ \text{PPMU(np)} \cdot I_{\mathrm{ft}^{\mathrm{l}}} \\ \text{PPMU(np)} \cdot I_{\mathrm{tf}^{\mathrm{nl}}} \end{bmatrix}}_{\mathrm{cc}} \begin{matrix} 1 \\ 2 \\ 3 \\ \vdots \\ \vdots \\ m_{k-1} \\ m_k \end{matrix} \tag{33}$$

The elements of $\mathscr{H}$ matrix is obtained corresponding to the voltage measurements of the $\boldsymbol{X}$ vector are obtained as

$$\mathscr{H}(i, n_{\mathrm{p}}(i)) = \mathscr{H}(i, n_{\mathrm{p}}(i)) - \frac{Y_{\mathrm{F}}(\mathrm{PMU}(n_{\mathrm{p}}(i)) \,.\, x(\mathrm{lid}, 1), n_{\mathrm{p}}(i))}{Y_{\mathrm{F}}(\mathrm{PMU}(n_{\mathrm{p}}(i)) \,.\, x(\mathrm{lid}, 1), \mathrm{PMU}(n_{\mathrm{p}}(i)) \,.\, z1(\mathrm{lid}, 1))} \tag{34}$$

$$\mathscr{H}(i, \mathrm{cc}(i)) = \frac{1}{Y_{\mathrm{F}}(\mathrm{PMU}(n_{\mathrm{p}}(i)) \,.\, x(\mathrm{lid}, 1), \mathrm{PMU}(n_{\mathrm{p}}(i)) \,.\, z1(\mathrm{lid}, 1))} \tag{35}$$

The various structure fields of PMUs and their accessing methods used in (34) and (35) are given in Tables 2–4.

Table 2 Structure field and accessing method of PMU

PMU	Parameter	Accessing method	Variable	Identifier used
Structure Field	id	PMU(1).id	PMU location	n_p
	x	PMU(1).*x*	lines/branches connected at PMU bus	*lid*
	*z*1	PMU(1).*z*1	far end bus of branches connected at PMU bus	NA
	I	PMU(1).I	line currents	NA
	V	PMU(1).V	PMU bus voltage	NA

Table 3 Structure field and accessing method of PMU(id)textitx

Accessing method	Accessed variable/parameter
PMU(1).*x*(1,1)	outbound/outgoing branch connected to PMU bus
PMU(1).*x*(2,1)	inbound/incoming branch connected to PMU bus
PMU(1).*x*(*lid*,1)	*lid*th branch connected to PMU bus

Table 4 Structure field and accessing method of PMU(id).*z*1

Accessing method	Accessed variable/parameter
PMU(1).*z*1(1,1)	far end bus of outbound/outgoing branch connected to PMU bus
PMU(1).*z*1(2,1)	far end bus of inbound/incoming branch connected to PMU bus
PMU(1).*z*1(lid,1)	far end bus of *lid*th branch connected to PMU bus

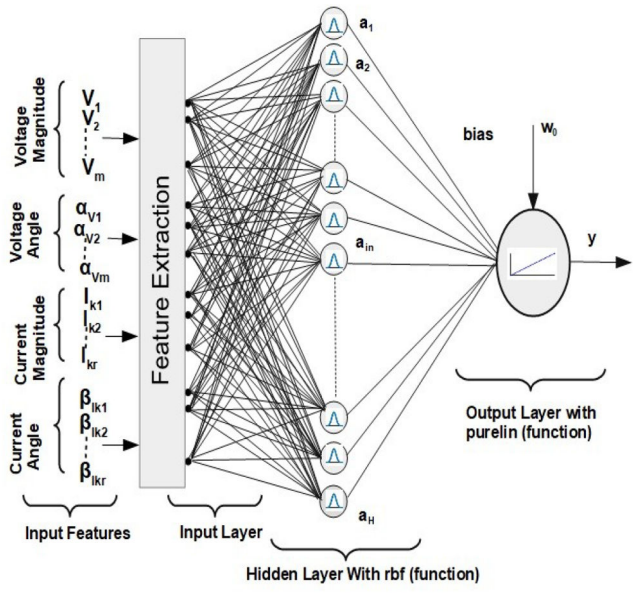

Fig. 6 *RBF architecture proposed*

5 Real-time estimation of ATC using ANN

5.1 Radial basis function neural network

Radial basis function network is a conglomeration of two types of neurons (radial basis feed forward neural network (RBF) and linear) arranged in three (input, hidden, and output) layers. The received input information is transmitted through the input layer to the next layer called the hidden layer. The hidden layer and output layer consist of RBF and linear neurons, respectively. The linear neurons are realised using a purelin transfer function. Each layer consists of several nodes that are fully connected to the relevant (preceding and/or succeeding) layer. Moore Penrose generalised pseudo-inverse method has been used to obtain the weights between hidden and output layers. The Moore Penrose method has been preferred over the other methods such as least mean square, linear least square regression etc. due to its shorter training time and generalisation ability. This property of the method makes it suitable for real-time applications, i.e. the present problem. The Gaussian kernel has been used as a radial basis function (for pattern recognition). The K-means clustering has been employed for determining the centre and width of the kernel.

5.2 ANN architecture

The architecture of ANN presented in this study has been given in Fig. 6. The RBF network architecture with the input set for the present problem has also been illustrated in the figure. The input to the network mainly consists of four different types of data, these data are voltage magnitude and angle of the buses at which the PMUs are located, branch currents, and branch current angles of the branches terminating or originating at the PMU location buses. If there are m PMU's optimally located in the system, then there will be m voltage magnitude $|V|$ inputs $(V_1, V_2, \ldots, V_m)$ and m voltage angle inputs V_a $(\alpha_{V_1}, \alpha_{V_2}, \ldots, \alpha_{V_m})$. Similarly if there are r branches terminating or originating at the kth PMU-bus then the branch current input of this unit would be $(I_{k1}, I_{k2}, \ldots, I_{kr})$ and branch current angles would be $(\beta_{I_{k1}}, \beta_{I_{k2}}, \ldots, \beta_{I_{kr}})$ and in this fashion, the entire branch current and branch current angle information is fed as input as $(I_{11}, I_{12}, \ldots, I_{mr})$ and $(\beta_{I_{11}}, \beta_{I_{12}}, \ldots, \beta_{I_{mr}})$. The size of the input vector would be $2 * m + \sum_{i=1}^{m} 2r_i$. This vector is passed through the LSE for obtaining all the states of the system (an amalgam of measured variables from PMU buses and estimated variables by LSE). Output of the LSE, i.e. $|V|, \alpha_v, I, \beta_I$ is feature set $\mathscr{D}$, which comprises a large number of features. For efficient performance of ANN-based estimators, these large features sets have to be reduced to a feature set $\mathscr{D}^r$ capable of adequately representing the complete set of features.

The $\mathscr{D}^r$ set of reduced features discussed in Section 5.3 is used as input and the corresponding ATC value obtained using the pattern search optimisation is used as the target output. The training process involves the optimal determination of centre and width of the RBF neurons to meet the required criterion of error tolerance.

5.3 Feature extraction (FE)

FE is an unavoidable process that is to be performed when a large number of data features are present. Feature extraction involves mapping of input features (large number) to new output features (fewer numbers). In this study, a sparse filtering algorithm (SFA) extraction method is used for extracting the dominant features, which could be used as input to the ANN. The SFA begins with data matrix $\mathscr{D}$ having n rows and p columns, where they (rows, columns) represent observations and measurements, respectively. The algorithm then takes either an initial random p-by-q (required number of features) weight matrix $\mathscr{W}$ and minimises (36). The method shortens the initial feature set $\mathscr{D}$ to a smaller set $\mathscr{D}^r$ using matrix $\mathscr{W}$ obtained by SFA (36)

$$\min \sum_{i=1}^{m} \| \tilde{\mathscr{D}}^{r,i} \|_1 = \sum_{i=1}^{m} \left\| \frac{\tilde{\mathscr{D}}^{r,i}}{\| \tilde{\mathscr{D}}^{r,i} \|_2} \right\|_1 \tag{36}$$

To compute objective function (36), which depends on the n-by-p data matrix $\mathscr{D}$ and weight matrix $\mathscr{W}$ the procedure given in Table 5 has been employed. The schematic representation SFA method has been illustrated in Fig. 7.

Table 5 SFA for feature extraction

Stage	Description
Step 1	compute the n-by-q matrix $\mathscr{D} \times \mathscr{W}$ and using the approximate absolute value function $\psi(u) = \sqrt{u^2 + \varepsilon}$, obtain the matrix $\mathscr{D}^r$. ψ is a symmetric non-negative and smooth function, which approximates the absolute value function and ε has been taken as 10^{-8} [30]
Step 2	define normalised $\tilde{\mathscr{D}}^r(i,j)$ as $\tilde{\mathscr{D}}^r(i,j)(i,j) = \frac{\mathscr{D}^r(i,j)}{\| \mathscr{D}^r(j) \|}$, where $\mathscr{D}^r(j) = \sqrt{\sum_{i=1}^{n} \tilde{\mathscr{D}}^r(i,j)^2 + \varepsilon}$
step 3	define normalised $\hat{\mathscr{D}}^r(i,j)$ as $\hat{\mathscr{D}}^r(i,j) = \frac{\tilde{\mathscr{D}}^r(i,j)}{\| \tilde{\mathscr{D}}^r(i) \|}$, where $\left\| \tilde{\mathscr{D}}^r(i) \right\| = \sqrt{\sum_{j=1}^{q} \tilde{\mathscr{D}}^r(i,j)^2 + \varepsilon}$
step 4	compute the objective function $h(\mathscr{W})$ as the 1-norm of the matrix $\hat{\mathscr{D}}^r(i,j)$ using $h(\mathscr{W}) = \sum_{j=1}^{q} \sum_{i=1}^{n} \hat{\mathscr{D}}^r(i,j)$
step 5	obtain the optimal value $\mathscr{W}$ using suitable techniques. Here, Broyden–Fletcher–Goldfarb–Shanno quasi-Newton optimiser has been employed [31] with termination criterion as the maximum number of iterations and step tolerance (if the norm of the algorithm step at any time is less than the specified tolerance).

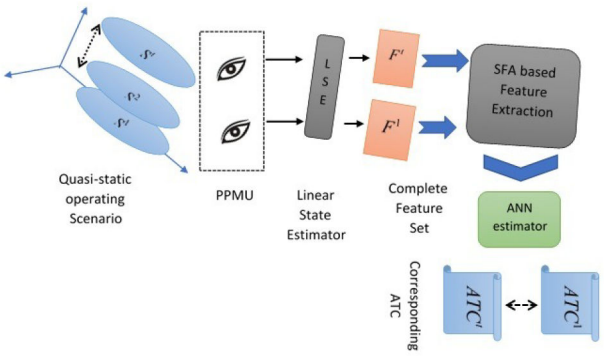

Fig. 7 *Schematic representation for feature extraction*

5.4 Testing

A part of the data archived for training is extracted and kept aside for training and validation of the trained neural network. If the desired goal of tolerance is met in the testing phase then the neural network is assumed to be trained and final weights and biasses are exported as a trained network, which could be used for real-time online estimation.

6 Implementation of the method

The software-based implementation of the proposed scheme has been depicted in Fig. 8*a* and practical hardware-based implementation has been shown in Fig. 8*b*. During software-based implementation there are apparently two different stages of the scheme: offline training and online implementation. The system scenario is inputted to the PSN solver, which is common to both online and offline stages. The PSN solver produces a solution corresponding to the input scenario and shares it with the PPMU emulator and optimisation engine simultaneously. The optimisation engine yields the optimal ATC values using the pattern search optimisation method discussed in this study and stores it in ATC storage. In ATC storage, the ATC values are stored sequentially to be used as target output to the neural network training block. Concurrently, the PPMU emulator interacts with the PSN solver to archive the voltages and currents of the PMU location buses and sends them to the LSE block. In the LSE block, all the states of the network are obtained. The LSE block sends the linearly estimated states to the ANN input block. It is to be clarified that the values sent by the ATC storage as target and the input sent by the nearest neighbour input block to the ANN are quasi-statically

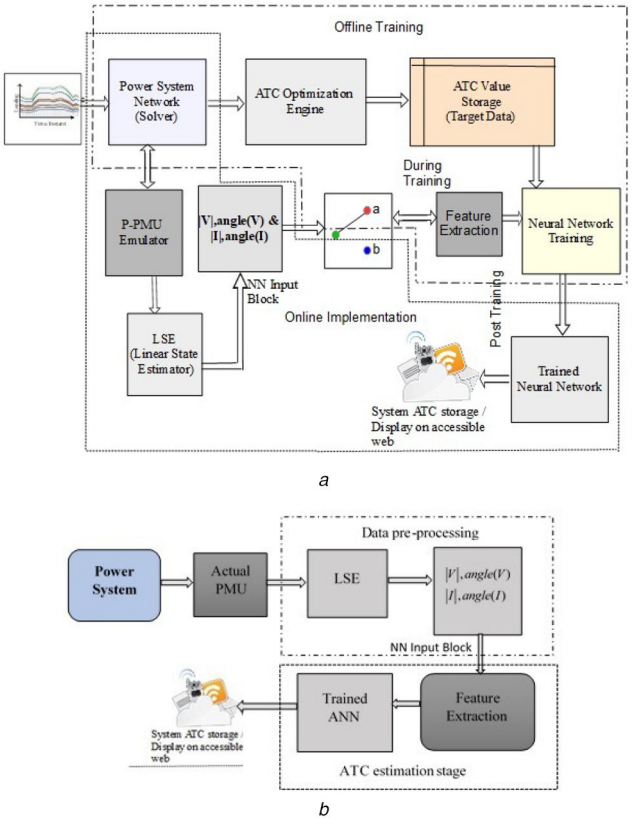

Fig. 8 *Schematic representation of the proposed method*
(a) Software-based development of proposed method, ***(b)*** Practical implementation layout of proposed method

synchronised. The ANN input block feeds the ANN training block until it is trained. This is depicted by placing the switch at position '*a*' of the switch block shown in Fig. 8*a*. The switch being in position '*b*' the trained ANN would produce ATC value for any novice input received from the ANN block. Once the network is trained, the final weights and biases are exported to the trained ANN block. This can be accomplished by diverting the switch from to position '*b*'. The ATC value so produced can be sent to the ATC storage for further applications such as power transaction management, forecasting, system analysis, display on publicly accessible web etc.

The above-described methodology can be practically implemented using trained ANN by a utility as shown in Fig. 8*b*. The PSN solver and input scenario have been replaced by the actual power grid whereas the PPMU emulator has been replaced by actual PMU in this figure. The PMU measurements have been directly sent to the data pre-processing stage (i.e. LSE and feature extraction) for ATC estimation by the trained ANN.

7 Authentication in real-time simulation using RTDS

Functioning of ANN estimator has been verified in real-time using RTDS platform. The test system has been modelled on RSCAD software and compiled on RTDS hardware. The different loading scenarios have been sent to the RTDS simulator from the monitoring and control center that has been build in MATLAB. The control center issues the appropriate command signals corresponding to any change in the operating scenario of the system. This communication is established through 'GTNET SKT' protocol. The 'GTNET SKT' protocol is capable of handling data streams with an update frequency of 2 kHz (maximum). A schematic representation of the process has been shown in Fig. 9.

The GTNET PMU has been placed at the optimal PMU locations in the power system model using RSCAD software. The RTDS uses the GTSYNC card to time stamp the measurement taken by the GTNET PMU's. These PMU's could publish data in the IEEE C37.118 protocol and send the data to other devices and

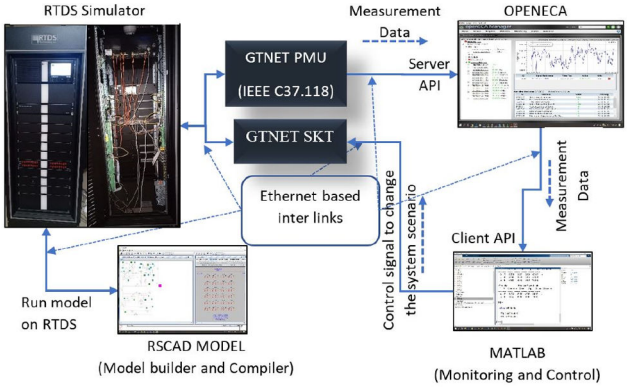

Fig. 9 *Pictorial illustration of the process used in authentication in RTDS simulation*

Table 6 Description of the test system

Case	Area	Generator bus	Load bus	PMU location bus (branch)	Gen cap, MW	Load, MW	Margin, MW
IEEE 24-bus test system	1	[14, 15, 16, 17, 18, 19, 21]	[5, 17, 19]	[16 (4), 21 (5)]	1170	1125	45
	2	[13, 22, 23]	[6, 8, 9, 10, 11, 12, 20]	[8 (3),10 (5), 23 (4)]	1551	1141	410
	3	[1, 2, 7]	[3, 4, 24]	[2 (3), 3 (3)]	684	584	100
IEEE 30-bus test system	1	[1,2]	[3, 4, 5, 6, 7, 8, 9, 11, 28]	[2 (4), 4 (4), 6 (7), 9 (3)]	121.94	84.5	37.44
	2	[13, 23]	[12, 14, 15, 16, 17, 18, 19, 20]	[12 (5), 15 (4), 19 (2)]	40	76.2	-36.2
	3	[22,27]	[10, 21, 24, 25, 26, 29, 30]	[10 (6), 25 (3), 27 (4)]	105	48.5	56.5
IEEE 118-bus test system	1	[61, 62, 65, 66, 69, 70, 72, 73, 74, 76]	[60, 67, 75, 78, 79, 47]	taken from [36]	2468.2	599	2049.2
	2	[99, 100, 103, 104, 105, 107, 110, 112, 113, 116]	[98, 101, 102, 106, 108, 109, 114, 115, 117, 118]	taken from [36]	1229.2	715	577

Table 7 Details of test cases under consideration (base case)

	Tie line	
Area	24-bus system	30-bus system
1 to 2	21–22, 17–22, 19–20(2), 14–11	4–12,
1 to 3	15–24	9–10, 6–10, 28–27
2 to 3	3–9, 4–9, 1–5, 2–6, 7–8	17–10, 20–10, 23–24

Table 8 Reduced features for different test cases using SFA

S.N	Test system	After PPMU		After LSE		Reduced feature
		[V, α, I, β]	[V & I]	[V, α, I, β]	V & I	
1	24	68	34	124	62	7
2	30	120	60	140	70	10
3	118	342	171	608	304	33

applications such as PDC. An open source PMU connection tester provided by grid protection alliance [32] has been used to test and generate PMU configuration files. These configuration files are used by the openECA to establish a connection with GTNET PMU and acquire measurement data using server API. The openECA sends the data to the monitoring and control center using the client API. The ATC estimator running in the monitoring and control center has been used to estimate the ATC in real-time.

8 Case study

The methods proposed in this study have been simulated on Intel core i7@2.24 GHz computer using MATLAB 2017b and MATPOWER 6.01 software. The description of the tests systems on which the proposed methods have been illustrated is delineated in the following subsystem.

8.1 Description of test system

The performance of the method has been manifested on IEEE 24-, 30-, and 118-bus systems. The data used for modified IEEE 24-, 30-, and 118-bus test systems have been taken from [33–35], respectively. Table 6 contains the information pertinent to the area wise classification of buses (both generator and load buses), optimal location of PMU's, the number of branches linked with the corresponding PMU buses (given in small bracket alongside the PMU bus location) along with the area wise generation capacity, load, and the available generation margin. The generation margin is an indicator that reflects the amount of power which an area can additionally supply to its own area without importing from other areas (while fulfilling the system criterion). The tie lines interconnecting the different areas are given in Table 7.

8.2 Result and discussion

For every input scenario (loads, generation, network topology, and PMU location) different values of TTC, corresponding to various contingencies have been obtained. These TTC values correspond to the minimum of the voltage, stability, and thermal limits. The TTC value corresponding to the severe-most contingency would be lowest. For a defined credible set of contingencies, a TTC ranking has been obtained and the top-ranking TTC value has been used to obtain ATC. Such a selection (TTC rank 1) for ATC calculation would guarantee the safer operation of the power system as any other single outage contingency would result into a TTC/ATC higher than the rank 1 selection.

8.2.1 Feature extraction: The result of feature extraction using the method discussed in Section 5.3 has been obtained for all the three test cases under study as tabulated in Table 8. The SFA has been used to reduce the size of the input features. The size of the reduced feature set is equal to the number of optimal PMU's that would be required for ensuring the complete observability of the system.

Table 9 Comparison of results obtained from TSCOPF and proposed method

Case description	Proposed method			TSCOPF [33]		
Outage	TTC, MW	CBM, MW	ATC, MW	TTC, MW	CBM, MW	ATC, MW
largest gen in area 1	465	–		350	–	–
largest gen in area 2	358.636	60	298.636	262.8	60	200.8
line 21–22	465	–		350	–	–
line 17–22	465	–		350	–	–
line 19–20	465	–		350	–	–
line 14–1	400	–		306.6	–	–

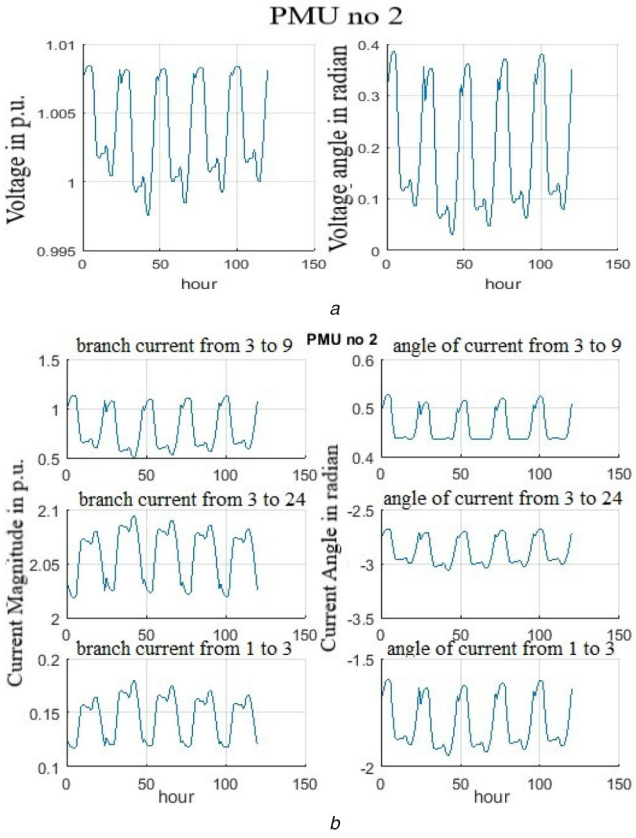

Fig. 10 *Data archived by PMU at bus 2*
(a) Voltage and voltage angle plot obtained by PMU 1 at bus 2, ***(b)*** Voltage and voltage angle plot obtained by PMU 1 at bus 2

8.2.2 Modified IEEE 24-bus RTS system: The entire network has been divided into three areas. The ATC for transfer of power from area 1 to area 2 has been evaluated using the proposed method. The CBM and TRM have been taken as 5% of the existing transmission commitments. The results obtained by the proposed method have been tabulated in Table 9 along with results reported in [33] for comparison. The TTC value corresponding to the contingency that yields the lowest TTC has been considered for ATC evaluation. Such a TTC value corresponds to the outage of the largest outage generator in area 2. It can be noticed from this table that the TTC corresponding to the above contingency produced by the proposed method is higher than the method reported in [33]. In other cases also the TTC is higher than the proposed method. The ATC has been calculated by taking CBM to be 60 MW as taken in [33] and tabulated in Table 9. The TRM is neglected for comparison of the proposed method with transmission security constrained optimal power flow (TSCOPF). It can be observed that the proposed method results in a higher value of ATC than that of the TSCOPF method [33].

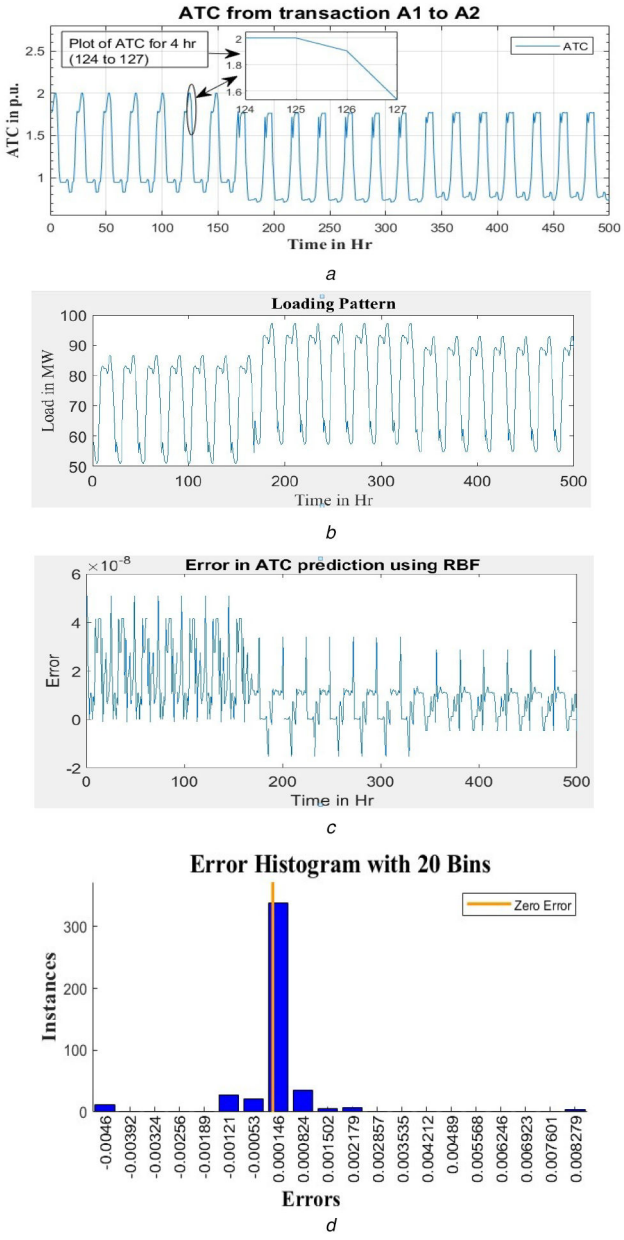

Fig. 11 *IEEE 24-bus test system emulation results*
(a) ATC from areas 1 to 2 for modified IEEE 24-bus test, ***(b)*** Loading pattern of modified IEEE 24-bus system, ***(c)*** Error in ATC prediction using ANN, ***(d)*** Error histogram of ATC estimator using reduced features for IEEE 24-bus system

The PMU emulation for the modified IEEE 24-bus system has also been done and the results obtained by PMU 2 (for example) are given in Fig. 10*a* and *b*. The figures show the voltage and current magnitudes and angles recorded by the PMU's as the system is subjected to the predefined loading pattern. PMU's are assumed to be placed at optimal locations with maximum observability as the objective of their placement. The optimal locations of the PMU in this work are taken from reference [37] and are given in Table 7. It can be observed from Fig. 10*a* and *b* that hourly load pattern has been quasi-statically simulated and the data archived by the PPMU emulator for 120 h are shown. The variations in the voltage and currents obtained are in phase with the variations observed in the loading for the same duration.

During the offline simulation stage, the ATC optimisation engine evaluated the ATC value corresponding to each loading scenario, and the corresponding value has been stored in the system ATC storage. Fig. 11*a* depicts the plot of ATC in the system from area 1 to area 2 without considering any outage in the system and Fig. 11*b* depicts the corresponding loading pattern. The data archived from the ATC storage system and PMU emulator has been used for the training of RBF- and levenberg-marquardt neural

Table 10 Condition of source and sink areas of 30-bus test system

Sl. No.	Parameter	Area	
		Area 1	Area 2
1	initial generation	84.51 MW	56.2 MW
2	max generation	160 MW	70 MW
3	available generation capacity	75.49 MW	13.8 MW
4	contingency considered	outage of generater at bus 23	

network-based neural networks. There are 68 inputs and a single output (ATC values) being used for training purposes, the inputs are obtained from the PMU emulator and comprises (V [magnitude and angle], branch currents [magnitude and angles]). The emulation has been done for a hourly load model given in reference [38]. The performance of the RBF neural network-based estimator for considered test system has been given in Fig. 11*c*. It can be observed that the error in ATC prediction is less in the case of the RBF neural network, and therefore RBF-based neural network ATC estimator has been proposed. The trained estimator has been used in real-time estimation of ATC. The input to the estimator is the voltages and current measured by the PPMU's across the system.

8.2.3 Modified IEEE 30-bus test system: The IEEE 30-bus system has been divided into three areas and ATC for the transaction of power between the areas has been evaluated. The input data has been randomly generated using uniform distribution between 80 and 120 percentages of base case loading by employing the equations given hereunder

$$P_L^i = P_L^0(1+\zeta) \tag{37}$$

$$Q_L^i = Q_L^0(1+\zeta) \tag{38}$$

Here, $\zeta = a + \text{rand}(b-a)$, $b = 0.2$ and $a = -0.2$.

The data generation is done by ensuring the fixed loading characteristics, which is achieved by maintaining a constant power factor. The condition and convergence of ATC optimisation engine for transfer from area 1 to area 2 have been given hereunder in Table 10 and in Fig. 12, respectively. It could be observed that PS converged in five iterations with -0.70677 as the best function value and 816 function evaluations.

In case of the IEEE 30-bus test system, the input scenarios have been generated by employing (3) and (38). The data archived by the PPMU emulator when the generated scenarios are quasi-statically simulated are given in Fig. 13. Fig. 13*a* depicts the voltage plot and Fig. 13*b* depicts the branch current plot. The ATC estimator for the IEEE 30 bus test system has been trained for quasi-static yearly data generated using loading factors given in [38]. The results of ATC estimation and corresponding error are given in Fig. 14.

8.2.4 Modified IEEE 118-bus test system: The IEEE 118 bus test has been modified by taking the long term line limit as ($2 \times$ base case power flow) and emergency rating as ($5 \times$ base case power flow). Furthermore, for the purpose of analysis, two different areas (area 1) and (area 2) comprising the buses given in Table 7 are formed. The ATC estimation for transaction from area 1 as the source and area 2 as the sink have been performed using the proposed method. The yearly loading factors given in [38] have been used to generate quasi-static data for the IEEE 118-bus test system. The 118-bus system being a large test case with a larger number of PMU's (n_p is 33). The size of the input to the ANN increased significantly. Therefore a feature extraction and selection method has been adopted to adequately train the ANN estimator. The input provided by the PPMU through LSE is (608×1), which is reduced to (33×1). The estimated ATC by the ANN estimator and its performance in terms of error has been given in Fig 15*a* and *b*.

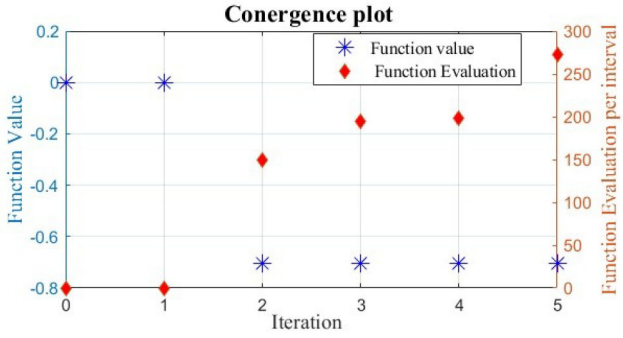

Fig. 12 *Plot of convergence for ATC evaluation of IEEE 30-bus test system from area 1 to area 2*

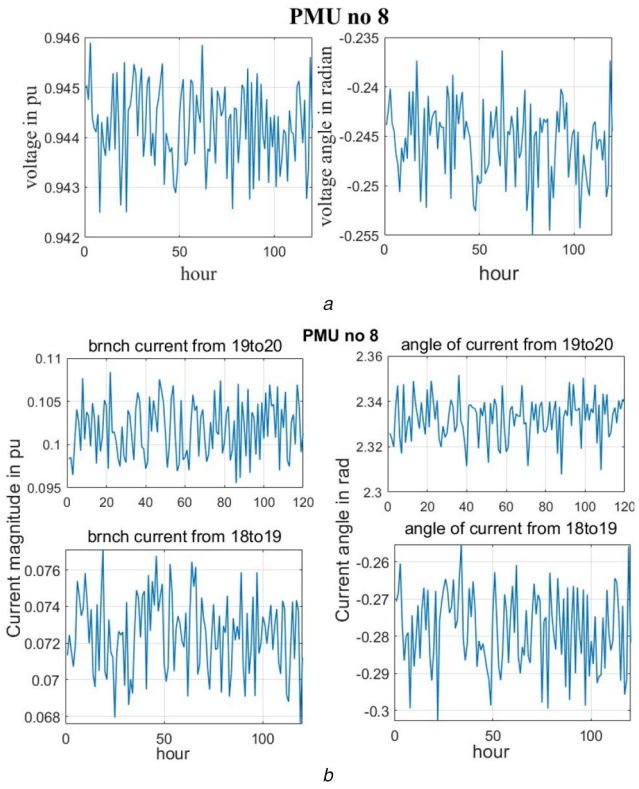

Fig. 13 *PMU emulation for IEEE 30-bus test system*
(a) Voltage and voltage angle plot obtained by PMU 8 at bus 19, ***(b)*** Branch current and angle plot obtained by PMU 8 at bus 19

8.2.5 Performance of ANN-based estimator: Comparative analysis of the developed estimator for different test system has been illustrated in Table 11. Here the error has been expressed in terms of mean absolute error (MAE), mean squared error (MSE), sum of absolute errors (SAEs) and sum of squared errors (SSEs). The sample size for obtaining the performance has been taken as 1000. It can be observed that after using the reduced feature set as input to the estimator, the error metrics deteriorated significantly but they are still under the acceptable limits. It has been noted that for the IEEE 118-bus test system, the error is more than the other two cases thus it can be said that the overall performance of the ATC estimator degrades with an increase in the complexity of the system. Nevertheless, the error falls well within the range of 10^{-3} to 10^{-5} which can be very well accepted for ATC estimation application. The overall time elapsed in data generation for ANN training, in ANN training, and ATC estimation have been given in Tables 12 and 13. The time elapsed have been acquired for solution obtained using the proposed method on MATLAB 2017b using Intel core i7 processor.

8.2.6 Real-time authentication of IEEE 30-bus test system using RTDS: The IEEE 30-bus test system has been modelled in

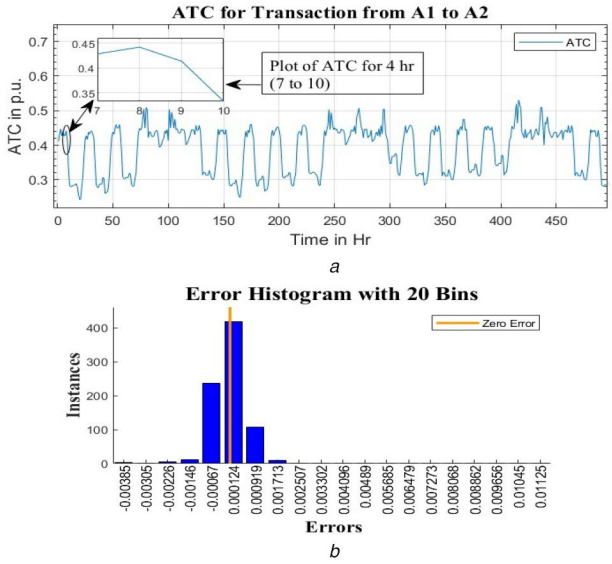

Fig. 14 *Result of ATC estimator for IEEE 30 bus test system*
(a) ATC estimated using ANN estimator for transaction from area 1 to area 2 of IEEE 30-bus system, ***(b)*** Error histogram of ATC estimator using reduced features for IEEE 30-bus system

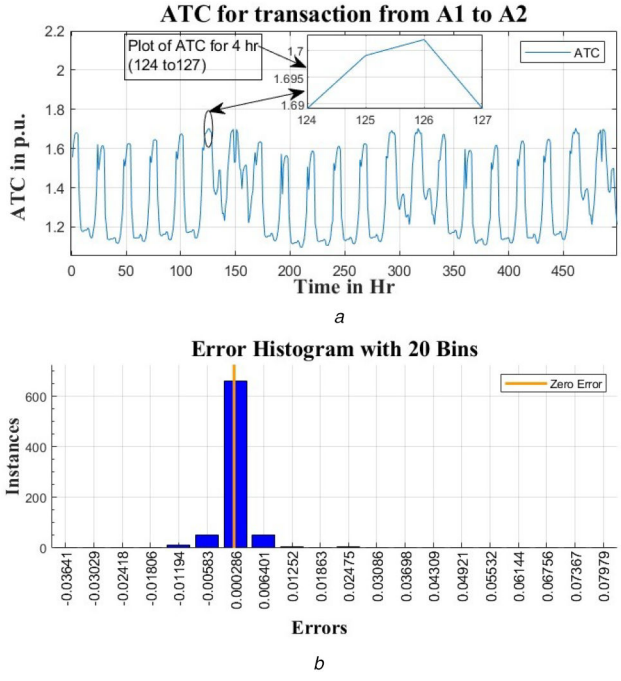

Fig. 15 *Result of ATC estimator for IEEE 118 bus test system*
(a) ATC estimated using ANN estimator for transaction from area 1 to area 2 of IEEE 118-bus system, ***(b)*** Error histogram of ATC estimator using reduced features for IEEE 118-bus system

Table 11 Performance of ANN estimator

S.N	Indices	Test cases					
		IEEE 24-bus		IEEE 30-bus		IEEE 118-bus	
		Before FE	After FE	Before FE	After FE	Before FE	After FE
1	MAE	2.10×10^{-8}	2.54×10^{-4}	7.42×10^{-4}	4.20×10^{-3}	1.76×10^{-4}	2.4×10^{-3}
2	MSE	1.51×10^{-15}	9.98×10^{-7}	3.87×10^{-6}	5.47×10^{-5}	1.21×10^{-7}	3.7×10^{-5}
3	SAE	1.55×10^{-3}	0.11	0.59	3.33	0.14	1.9
4	SSE	6.81×10^{-13}	4.49×10^{-4}	3.10×10^{-3}	4.38×10^{-2}	9.65×10^{-5}	2.90×10^{-2}

RTDS software. The system has been subjected to different loading scenarios using the command signals issued from the control center through the GTNET SKT. The 'GTNET PMU's have been used to measure the relevant parameters. These PMU measurements have been acquired using the IEEE C.37.118 protocol by 'openECA' software. These measurements have been sent to the control center where the proposed method has been utilised to estimate the ATC. The overall time elapsed in various processes during the ATC estimation has been given in Table 14 The result of estimated ATC values and corresponding loading scenario has been shown in figures Fig. 16*a* and Fig. 16*b*. The loading pattern has been changed at the interval of 40 s. The corresponding ATC values

Table 12 Training time and data generation time

Test system	Data generation time, s		ANN training time, s	
	Duration	Time	Without FE	With FE
24-bus	8760	43800.51	13.21	9.54
30-bus	8760	70080.43	68.03	47.5
118-bus	8760	91980.29	94.47	72.7

Table 13 Offline training and testing time

	Without feature extraction			
Test System	Training time	Estimator time	LSE time	Total time
24-bus	13.21	6.85×10^{-3}	1.98×10^{-4}	7.05×10^{-3}
30-bus	68.03	7.80×10^{-3}	2.99×10^{-4}	8.10×10^{-3}
118-bus	94.47	8.86×10^{-3}	3.01×10^{-4}	9.16×10^{-3}

	With feature extraction				
Test system	Training time	FE time	Estimator time	LSE time	Total time
24-bus	9.54	4.71×10^{-4}	5.80×10^{-3}	1.98×10^{-4}	6.00×10^{-3}
30-bus	47.5	4.38×10^{-4}	7.70×10^{-3}	2.99×10^{-4}	8.00×10^{-3}
118-bus	72.7	4.60×10^{-4}	7.18×10^{-3}	3.01×10^{-4}	7.48×10^{-3}

Table 14 Real-time implementation on RTDS

Test system	Communication time, s	LSE time, s	FE time, s	Estimation time, s	Total time, s
IEEE 30 bus	5.00×10^{-2}	7.80×10^{-3}	2.99×10^{-4}	$7.70 \times 10-3$	6.58×10^{-2}

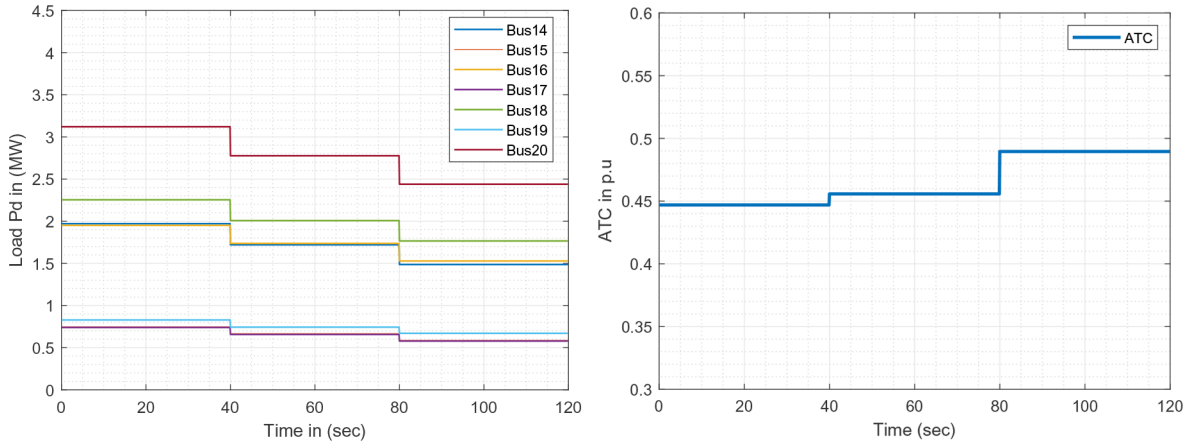

Fig. 16 *Estimated ATC and loading of buses in area A2 during RTDS simulation*
(a) Loading of buses in area A2, ***(b)*** ATC estimated using proposed ATC estimator

Table 15 Comparison of proposed method with the referred methods

System	Source	Sink	Referred method		Proposed method
			SATC, MW	DATC, MW	ATC, MW
30-bus [39]	2	18	3.7	0.95	3.86
	2	23	3.6	1.15	3.95
	2	30	2.09	0.63	2.0974
39-bus [40]	36	21	–	7.3	20.0000
145-bus [39]	141–143	34, 35	6.5	1.82	6.5478

have been shown in Fig. 16*b*. It can be observed from these results that the ATC values increases with a decrease in load.

8.2.7 ATC and dynamic ATC: The dynamic ATC for a system for any transaction can be considered as an approximation of the static ATC [39]. A comparative analysis of static and dynamic ATC has been done for different cases and reported in Table 15. It can be observed that the ATC obtained using the proposed method is three to four times the dynamic ATC.

9 Conclusion

A framework for real-time ATC estimation using ANN has been presented with its application on IEEE 24-bus, IEEE 30-bus, and IEEE 118-bus test systems. An ATC optimisation engine

employing the proposed method for estimation of ATC has been used for obtaining the ATC training data in the offline stage of real-time estimator development. A PMU emulation algorithm for quasi-static analysis of power system (using PPMU) has been developed and used to obtain the voltage and current states of the system quasi-statically. The information obtained from the PPMU's has been used as an input of the real-time ATC estimator. The results have been authenticated using a RTDS on the IEEE 30-bus test system.

10 Acknowledgments

The authors acknowledge the support provided under R&D Grant Vide Letter IIT(BHU)/R&D/Lab Grant/2018-19/4161/L dated 16/1/2019 through the project 'Real Time Simulation of Smart Grid with Distributed Energy Resources under.'

11 References

[1] Ejebe, G.C., Tong, J., Waight, J.G., *et al.*: 'Available transfer capability calculations', *IEEE Trans. Power Syst.*, 1998, **13**, (4), pp. 1521–1527

[2] Chiang, H.D., Li, H.: '*On-line ATC evaluation for large-scale power systems: framework and tool*' (Springer, Boston, MA, USA, 2005), pp. 63–103. Available at https://doi.org/10.1007/0-387-23471-3_5

[3] Force, T.T.C.T., Available transfer capability definitions and determination, report, North American Electric Reliability Council (NERC) Report, Princeton, NJ, 1996

[4] Ma, J., Zhang, P., Fu, H.j., *et al.*: 'Application of phasor measurement unit on locating disturbance source for low-frequency oscillation', *IEEE Trans. Smart Grid*, 2010, **1**, (3), pp. 340–346

[5] Cui, B., Srivastava, A., Banerjee, P.: 'Synchrophasor based condition monitoring of instrument transformers using clustering approach', *IEEE Trans. Smart Grid*, 2019, **11**, (3), pp. 2688–2698

[6] Lin, J., Song, J., Lu, C.: 'Synchrophasor data analytics: transmission line parameters online estimation for energy management', *IEEE Trans. Eng. Manage.*, 2019. Early Access, doi: 10.1109/TEM.2019.2939173

[7] Panda, R.K., Mohapatra, A., Srivastava, S.C.: 'Online estimation of system inertia in a power network utilizing synchrophasor measurements', *IEEE Trans. Power Syst.*, 2019, **35**, (4), pp. 3122–3132

[8] Ghawghawe, N.D., Thakre, K.L.: 'ATC evaluation with consideration of load changes and participation factors – a sensitivity analysis approach'. 2007 Int. Power Engineering Conf. (IPEC 2007), Singapore, 2007, pp. 124–129

[9] Kumar, J., Kumar, A.: 'ACPTDF for multi-transactions and ATC determination in deregulated markets', *Int. J. Electr. Comput. Eng.*, 2011, **1**, (1), pp. 71–84

[10] Chen, Z., Zhou, M., Li, G.: 'ATC determination for the ac/dc transmission systems using modified CPF method'. 2010 5th Int. Conf. on Critical Infrastructure (CRIS), Beijing, People's Republic of China, 2010, pp. 1–8

[11] Yuan, Y., Kubokawa, J., Nagata, T., *et al.*: 'A solution of dynamic available transfer capability by means of stability constrained optimal power flow'. 2003 IEEE Bologna PowerTech – Conf. Proc., Bologna, Italy, 2003, vol. 2, pp. 191–198

[12] Li, G., Sun, H., Lv, Z.: 'Study of available transfer capability based on improved artificial fish swarm algorithm'. 2008 Third Int. Conf. on Electric Utility Deregulation and Restructuring and Power Technologies, Nanjing, People's Republic of China, 2008, pp. 999–1003

[13] Bavithra, K., Raja, S.C., Venkatesh, P.: 'Optimal setting of facts devices using particle swarm optimization for ATC enhancement in deregulated power system', *IFAC-PapersOnLine*, **49**, (1), pp. 450–455. 4th IFAC Conference on Advances in Control and Optimization of Dynamical Systems ACODS 2016. Available at http://www.sciencedirect.com/science/article/pii/S2405896316300957

[14] Shukla, D., Lakshmi, E.S., Singh, S.P.: 'Estimation of ATC using PS-NR'. 2017 6th Int. Conf. on Computer Applications In Electrical Engineering-Recent Advances (CERA), Roorkee, India, 2017, pp. 111–116

[15] Cheng, H., Zheng, Y., Li, F., *et al.*: 'Probabilistic assessment of interregional available transfer capability for renewable energy transactions'. 5th Int. Conf. on Electric utility Deregulation and Restructuring and Power Technologies (DRPT), Changsha, People's Republic of China, 2015, pp. 76–81

[16] Patton, A.D., Luo, X., Singh, C.: 'Real power transfer capability calculations using multi-layer feed-forward neural networks', *IEEE Trans Power Syst.*, 2000, **15**, (2), pp. 903–908

[17] Jain, T., Singh, S.N., Srivastava, S.C.: 'A neural network based method for fast ATC estimation in electricity market'. IEEE PES General Meeting, Tampa, FL, USA, 2007, pp. 1–8

[18] Pandey, S.N., Pandey, N.K., Tapaswi, S., *et al.*: 'Neural network based approach for ATC estimation using distributed computing', *IEEE Trans. Power Syst.*, 2010, **25**, (3), pp. 1291–1300

[19] Jain, T., Singh, S.N., Srivastava, S.C.: 'Fast static available transfer capability determination using radial basis function neural network', *Appl. Soft Comput.*, 2011, **11**, pp. 2756–2764

[20] Kesherwani, S., Srivastava, S.C., Mohapatra, A.: 'Synchrophasor measurement-based approach for online available transfer capability evaluation', *IET Gener. Trans. Distrib.*, 2019, **13**, (17), pp. 3941–3950

[21] Chen, H., Fang, X., Zhang, R., *et al.*: 'Available transfer capability evaluation in a deregulated electricity market considering correlated wind power', *IET Gener. Trans. Distrib.*, 2018, **12**, (1), pp. 53–61

[22] Wang, S., Gao, S.: 'Available transfer capability analysis method of AC-DC power system based on security region', *J. Eng.*, 2019, **2019**, (16), pp. 2386–2390

[23] Avila, N.F., Chu, C.: 'Distributed probabilistic ATC assessment by optimality conditions decomposition and LHS considering intermittent wind power generation', *IEEE Trans. Sust. Energy*, 2019, **10**, (1), pp. 375–385

[24] Mohammed, O.O., Mustafa, M.W., Mohammed, D.S.S., *et al.*: 'Available transfer capability calculation methods: a comprehensive review', *Int. Trans. Electr. Energy Syst.*, 2019, **29**, (6), pp. e2846. Available from: https://onlinelibrary.wiley.com/doi/abs/10.1002/2050-7038.2846

[25] Audet, C., Dennis, J.E. Jr.: 'Analysis of generalized pattern searches', *SIAM J. Optim.*, 2003, **13**, (3), pp. 889–903

[26] Shukla, D.: 'Real time assessment of available transfer capability'. IIT (BHU) Varanasi, 2015

[27] Matlab Documentation Center – Mathworks India. Available at https://in.mathworks.com/help/search.html?submitsearch=&qdoc=patternsearch (accessed 24 January 2019)

[28] Sunitha, R., Kumar, R.S., Mathew, A.T.: 'Online static security assessment module using artificial neural networks', *IEEE Trans. Power Syst.*, 2013, **28**, (4), pp. 4328–4335

[29] Yang, T., Sun, H., Bose, A.: 'Transition to a two-level linear state estimator; part I: architecture', *IEEE Trans. Power Syst.*, 2011, **26**, (1), pp. 46–53

[30] Ngiam, J., Chen, Z., Bhaskar, S.A., *et al.*: 'Sparse filtering', *Adv. Neural Inf. Process. Syst.*, 2011, **24**, pp. 1125–1133

[31] Nocedal, J.: '*Numerical optimization (springer series in operations research)*' (Springer, 2006,2nd edn.)

[32] Alliance, G.P.: 'Open Source Software & Services for Electric Utilities'. Available at https://gridprotectionalliance.org/dev/default.asp, CA, USA

[33] Ou, Y., Singh, C.: 'Assessment of available transfer capability and margins', *IEEE Trans. Power Syst.*, 2002, **17**, (2), pp. 463–468

[34] Alsac, O., Stott, B.: 'Optimal load flow with steady-state security, power apparatus and systems', *IEEE Trans. Power Syst.*, 1974, **PAS-93**, (3), pp. 745–751

[35] Archive, U.: 'Power systems test case archive'. Available at 'http://www.ee.washington.edu/research/pstca/ Accessed December 2018

[36] Singh, S.P., Thakur, A.K., Singh, S.P.: 'PMU placement for maximum observability of power system under different contingencies', *Energy Procedia*, 2017, **117**, pp. 893–900

[37] Singh, S.P., Singh, S.P.: 'A multi-objective PMU placement method in power system via binary gravitational search algorithm', *Electr. Power Compon. Syst.*, 2017, **45**, (16), pp. 1832–1845. Available at https://doi.org/10.1080/15325008.2017.1378775

[38] Billinton, R., Li, W.: '*Reliability assessment of electric power system using system using monte carlo methods*' (Springer, New York, NY, USA, 1994)

[39] Venkaiah, K.M.Ch., Vinod Kumar, D.M.: 'Dynamic ATC computation for real-time power markets', *J. Electr. Eng. Technol.*, 2010, **5**, (2), pp. 209–219

[40] Eidiani, M., Shanechi, M.H.M.: 'FAD-ATC: a new method for computing dynamic atc', *Int. J. Electr. Power Energy Syst.*, 2006, **28**, (2), pp. 109–118